Smart Structures and Systems, *Vol. 28, No. 4 (2021) 455-468*
https://doi.org/10.12989/sss.2021.28.4.455

Analysis, optimization and control of an adaptive tuned vibration absorber featuring magnetoactive materials

Fan Lin [1a], Masoud Hemmatian*[1], Ramin Sedaghati [1b] and Farhad Aghili [2c]

[1] *Department of Mechanical, Industrial and Aerospace Engineering Concordia University, Montreal, H3G 1M8, Canada*
[2] *John H. Chapman Space Center Canadian Space Agency, 6767 Route de l'Aéroport, Saint-Hubert, Québec, J3Y 8Y9, Canada*

(*Received May 12, 2020, Revised July 6, 2021, Accepted July 9, 2021*)

Abstract. Excessive vibration may cause premature fatigue failure on structural components if it is not properly controlled. One effective way to attenuate vibration is to attach a tuned vibration absorber to the main structural component. Passive tuned vibration absorbers are mainly effective to attenuate vibration at a specific range of frequencies and thus they become infective under varied environmental conditions which can significantly alter the tuning frequencies. The present study aims at development of a wide-bandwidth and light-weight adaptive tuned vibration absorber (ATVA) featuring a magnetorheological elastomer (MRE) which is tuned to absorb the vibrations of a flexible beam. The accelerance transfer function is derived for both beam with and without ATVA. The effectiveness of the ATVA to control vibration of the flexible beam caused by external excitation under wide range of frequencies is demonstrated. The proposed ATVA consists of C-Shape frame with winding coils, two isometric MRE specimens with 40% volume fraction, and active mass. An empirical model for the MRE has been developed through an experimental identification method in order to predict the MRE's elastic modulus under various levels of excitation frequencies and applied magnetic fields. Using MRE models and magneto-circuit analysis, the frequency bandwidth of the ATVA is analytically obtained. The analytical model is then used to develop a multidisciplinary design optimization formulation to minimize the mass and maximize the frequency bandwidth of an ATVA featuring MRE given several geometrical and physical constraints. Finally, a tuning algorithm has been presented to determine the required applied magnetic flux density to the MRE layers based on the identified phase difference between the absolute acceleration of the host and relative acceleration of the host and ATVA's resonator.

Keywords: adaptive tuned vibration absorber; design optimization; magnetorheological elastomer; vibration control

1. Introduction

Excessive vibration can potentially cause premature fatigue failure of mechanical and structural components that may result in catastrophic failure of whole system. Considering this, significant research studies have been conducted in the past few decades to develop design strategies to mitigate vibration. Dynamic vibration absorbers (DVAs) are one of the most widely secondary vibratory systems which are attached to the primary structural system to attenuate unwanted vibration in main structural and mechanical systems. DVAs are generally categorized into passive, active and semi-active systems. Numerous research studies have been conducted on development, analysis and design optimization of passive DVAs to attenuate vibration at the desired tuned frequency. While passive vibration control strategy is a reliable and cost-effective approach, they are mainly effective to control vibration within a narrow frequency range which should be known formerly at early stages of design. The vibration control authority of passive DVAs significantly diminishes under mistuned conditions and may even worsen the condition by increasing the vibration level under mistuned conditions. Fully active DVAs utilize active control system to provide counteracting forces to attenuate system vibration using active actuators such as electromagnetic motors (e.g., solenoids, voice coils, etc.) or smart piezoelectric actuators based on measurement of system response. Fully active vibration control strategies are proven to have significant performance compared with passive systems as they are capable of providing the cancelling force to attenuate vibration under unpredicted environmental conditions. However, practical implementation of fully active systems is generally limited due to high cost associated with power requirements as well as complex control hardware. Moreover, active DVAs should be thoroughly verified for stability conditions as they apply energy to the system which may cause system destabilization. Semi-active strategies, on the other hand, have received considerable attention as they can provide reliability and fail-safe feature of passive DVAs while maintain the adaptability of the full active systems using low power and without requiring complex control hardware. Semi-active magnetorheological (MR) materials have recently provided a unique opportunity to develop semi-

*Corresponding author, Post-Doctoral Fellow,
E-mail: m_hemmat@encs.concordia.ca
[a] M.A.Sc. Student, E-mail: duoduolin0630@gmail.com
[b] Professor, E-mail: ramin.sedaghati@concordia.ca
[c] Research Scientist, E-mail: farhad.aghili@canada.ca

ISSN: 1738-1584 (Print), 1738-1991 (Online)

active MR-based adaptive DVAs which could be effectively integrated with host structures to attenuate vibration in wide range of frequencies (Ahamed *et al*. 2018). While semi-active DVA featuring MR fluids (MRFs) can provide variable damping in conventional tune vibration absorbers, semi-active DVAs featuring MR elastomers (MREs), which are called here adaptive tuned vibration absorbers (ATVAs), are capable of adjusting their resonance frequency to follow the excitation frequency by controlling the viscoelastic properties (elastic modulus) of MREs using applied magnetic field intensity (Skalski and Kalita 2017).

In recent years, MRE-based ATVAs have been used to attenuate vibration of primary systems in various applications including powertrain systems (Hoang *et al*. 2009, Qian *et al*. 2017, Gao *et al*. 2019), rotary system (Liu *et al*. 2017), structures (Deng *et al*. 2006, Deng and Gong 2008), and noise control (Hemmatian and Sedaghati 2016). In this subject, Deng *et al*. (2006) developed a shear mode ATVA using MRE. They demonstrated that varying electromagnet current from 0 to 1.5 A results in variation of the resonance frequency from 55 Hz to 81.25 Hz. Besides, Deng and Gong (2008) reported that an MRE-based ATVA under the shear mode can be tuned from 27.5 Hz to 40 Hz. Similar MRE-based ATVA was also developed by Zhang and Li (2009). The results indicated that the frequency can be altered from 35 Hz to 90 Hz. Ginder *et al*. (2001) constructed and tested tunable automotive mounts and bushings using MRE which could be applied to shift the suspension resonances away from the excitation frequency and minimize the effect of the resonances excited by torque variation of worn brake rotors. MREs have also been utilized in the development of variable-spring-rate elements for an ATVA. It was shown that the natural frequency of the ATVA can vary from 580 to 710 Hz under a magnetic field of 0.56 T (Ginder *et al*. 2002) demonstrating 22% shift in frequency from its zero-field condition. In addition to the MRE-based vibration absorbers operating in shear mode, the performance of the MREs operating in squeeze (tension-compression) or mixed (combination of shear and squeeze) modes were also investigated (Popp *et al*. 2009). Popp *et al*. (2009) compared the frequency shift of MRE-based vibration absorbers working under shear and squeeze mo2es and showed that the MR effect is higher in the case of squeeze mode. Similarly, Zhang *et al*. (2008), Lerner and Cunefare (2008), and Hwang *et al*. (2020) demonstrated that MREs working in a squeeze mode could greatly enhance the MR effect.

While the application of MREs in the development of ATVAs have been investigated in few studies, none of them presented the multidisciplinary design optimization of MRE-based ATVAs. The present study aims at the development, design optimization and control of an MRE-based ATVA operating in shear mode to be attached to a simply-support structural beam as the main system and attenuate its vibration under tonal excitation. For this purpose, the accelerance transfer function of the beam at midpoint is formulated which will be subsequently used for the analysis of the efficiency of the ATVA in vibration attenuation of the beam as the host structure. Moreover, the viscoelastic properties of the MRE are characterized experimentally by conducting oscillatory shear test under varying excitation and magnetic field intensity and a material model is developed to predict the variation of the storage and loss moduli with respect to the applied magnetic field and excitation frequency. The applied magnetic flux density as well as the variation in the natural frequency of the MRE-based ATVA are formulated as a function of geometrical and magnetic circuit parameters. The model is then utilized to formulate the design optimization strategy to maximize the frequency bandwidth of the developed absorber subject to size, weight and magnetic circuit constraints. Subsequently, the optimization problem is solved using the gradient based sequential quadratic programing (SQP) technique. Finally, a tuning controller is developed to evaluate the performance of the optimized MRE-based ATVA in the frequency range of interest. The phase difference between the absolute acceleration of the host and the relative acceleration of the host and absorber's resonator is identified and used in the control law to determine the required magnetic flux density. The results are presented in both time and frequency domains and showed a considerable performance of the developed MRE-based ATVA operating using the tuning algorithm.

2. Modeling of simply supported beam with integrated ATVA

Fig. 1 shows the schematic of an elastic beam with simply supported boundary conditions. Using the Euler-Bernoulli theory, the shear deformation is considered negligible compared with the bending deformation. As shown in Fig. 1, a load, P(x,t), is uniformly applied to the beam. The generalized equation of motion of the beam can be described as (Thomson and Dahleh 1998)

$$\frac{\partial^2}{\partial x^2}\left[E_b I_b(x)\frac{\partial^2 w(x,t)}{\partial x^2}\right] + \rho_b \bar{A}_b(x)\frac{d^2 w(x,t)}{dt^2} = P(x,t) \quad (1)$$

where E_b is the young's modulus of the beam, $I_b(x)$ is the second moment of the area of the cross section about the neutral axis through its centroid, $\bar{A}_b$ is the area of the cross section, and ρ_b is the mass density.

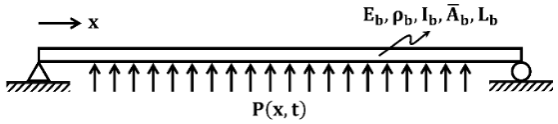

Fig. 1 Schematic of a simply supported beam with generalized force

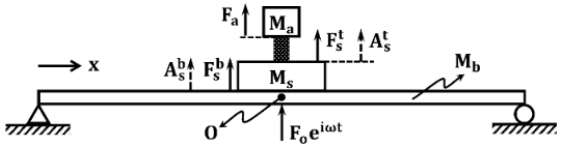

Fig. 2 Schematic of a simply-supported beam integrated with ATVA at the midpoint

To evaluate the frequency response of the system, accelerance transfer function (ratio of output acceleration to input force) at driving point x, H_x, has been derived. We can write

$$H_x = \frac{A_x}{F_x} \tag{1}$$

where A_x is the output acceleration, and F_x is the input force at driving point x. It is noted that the accelerance is basically the inverse of the apparent mass. As the frequency increases the apparent mass should approach to the inverse of the static mass of the system.

The accelerance function at the mid span can be obtained by dividing the acceleration by the force applied at mid span, $F(S) = F_o^b(j\omega)$, as follows (Deng *et al*. 2006, Lin 2019)

$$H_O^b = \frac{A_O^b}{F_O^b} = -\omega^2 \sum_{i=1}^{n} \frac{\phi_i^2}{M_i(\omega_k^2(1 + j\eta_b) - \omega^2)} \tag{3}$$

Where F_O^b and A_O^b are the amplitude of the excitation force and the acceleration at point O, respectively. ω_k and ϕ_k are the kth natural frequency and mode function of the beam, respectively, and n is the number of the mode which is taken into account. η_b is the loss factor of the beam and ω is the angular frequency of the excitation force.

For the simply supported beam, the normal mode functions and undamped natural frequencies can be obtained as (Thomson and Dahleh 1998)

$$\phi_n(x) = \sqrt{2}\sin\frac{n\pi x}{L_b} \tag{4}$$

Where L_b is the length of the beam. Using the normal modes and assuming uniform mass density, $m(x) = \frac{M_b}{L_b}$, M_i is obtained as follows

$$M_i = \frac{M_b}{L_b}\int_0^L 2\left(\sin\frac{n\pi x}{L_b}\right)^2 dx = M_b \tag{5}$$

It is note that dynamic response is usually dominated by the first few modes.

Fig. 2 shows a schematic diagram in which an ATVA is integrated at the midpoint of the simply supported beam. where M_a and M_s are the mass of ATVA's oscillator and the mass of ATVA's body including the electromagnet wires and core, respectively. M_b is the static mass of the beam. An excitation force which causes the oscillation is noted as $F_o e^{iwt}$ and the opposite reaction force that the ATVA applying on the beam is denoted as F_s^b. In addition, the resulting force at the upper surface of the core mass M_s given as F_s^t and F_a indicates the force exerted by the equivalent stiffness of the ATVA.

Thus, the accelerance function at mid-span of the beam in the presence of ATVA can be written as following for the system integrated with ATVA (Deng *et al*. 2006, Lin 2019)

$$A_o = H_o^b(F_o - F_s^b) \tag{6}$$

Since the core mass, M_s, is rigidly attached to the beam as shown in Fig. 2, the acceleration at the top, A_s^t, and bottom, A_s^b, of the mass would be the same and equal to the acceleration of the beam at the mid-point, A_0. In other words, we can write

$$A_s^b = A_s^t = A_o \tag{7}$$

Using Newton's law, the relation between forces and acceleration can be defined as

$$F_s^b + F_s^t = M_s A_s^t \tag{8}$$

As the mass of viscoelastic elements in ATVA is far less than the mass of the ATVA, it can be considered to be massless and due to equilibrium one may write

$$F_a = -F_s^t \tag{9}$$

in which absorber force, F_a, is determined using the acceleration of the absorber active mass, M_A, as

$$F_a = M_a A_a \tag{10}$$

Considering ATVA has a single DOF, the stiffness, K, of the absorber can be presented as $K = \omega_a^2 M_a$, in which ω_a is the frequency of the absorber. However, in terms of MRE-based ATVA, the MRE component possess both stiffness and damping which is typically represented as the complex stiffness, K^*, which can be defined as

$$K^* = K(1 + \eta j) \tag{11}$$

in which the K and η are the storage modules and loss factor of the MRE, respectively. It is noted that at the resonance frequency, the loss factor is equal to twice the equivalent viscous damping factor, ξ ($\eta = 2\xi$).

It is also noted that the absorber force, F_a, can be obtained from relative displacement of the MRE component as

$$F_a = K^*(w_a - w_s^t) = \frac{K^*}{\omega^2}(A_a - A_s^t) \tag{12}$$

in which w_a and w_s^t are the displacement of the active mass and displacement at the top of the core mass, respectively. Now substitution of Eqs. (9) and (10) into (8) and considering Eq. (7) yields

$$F_s^b = M_s A_o + M_a A_a \tag{13}$$

Eq. (10) can also be substituted into the Eq. (12) to obtain A_a as

$$A_a = \frac{K^* A_o}{K^* - \omega^2 M_a} \tag{14}$$

Finally substituting A_a from Eq. (14) into Eq. (13) yields

$$F_s^b = M_s A_o + M_a \times \frac{K^* A_o}{K^* - \omega^2 M_a} \tag{15}$$

Dividing both sides of Eq. (15) by A_o gives

$$R = \frac{F_s^b}{A_0} = M_s + M_a \times \frac{K^*}{K^* - \omega^2 M_a} \Longrightarrow F_s^b = RA_0 \quad (16)$$

Now substituting F_s^b from Eq. (16) into Eq. (6) yields the following relation for the acceleration of the beam at the mid-span, A_o

$$A_o = \frac{1}{1 + H_O^b R} H_O^b F_o \Longrightarrow A_o = \frac{\frac{1}{R}}{\frac{1}{R} + H_O^b} H_O^b F_o \quad (17)$$

As it can be realized, $1/R$ can be considered as the change in accelerance due to the existence of the ATVA; $\Delta H = 1/R$. Thus, Eq. (17) may be better described as (Deng *et al*. 2006, Lin 2019)

$$A_o = \frac{\Delta H}{H_O^b + \Delta H} H_O^b F_o \quad (18)$$

in which

$$\Delta H = 1/\left(M_s + M_a \times \frac{K^*}{K^* - \omega^2 M_a}\right) \quad (19)$$

where ΔH should be specified as the additional accelerance at the midpoint O due to the absorber. The modified accelerance transfer function for the beam with integrated ATVA is then denoted as, H_A, which can be mathematically expressed as follows (Deng *et al*. 2006, Lin 2019)

$$H_A = \frac{\Delta H}{H_O^b + \Delta H} H_O^b \quad (20)$$

It should be noted that in absence of an active mass, M_a, the accelerance of the system with integrated passive mass, M_s, at the midpoint O is defined as (Deng *et al*. 2006, Lin 2019)

$$H_S = \frac{\Delta H^r}{H_O^b + \Delta H^r} H_O^b \quad (21)$$

where ΔH^r is

$$\Delta H^r = 1/M_s \quad (22)$$

2.1 Response of the system without and with ATVA

For the proposed model of the beam integrated with an ATVA, it is necessary to verify the effectiveness of the absorber in vibration mitigation of the beam. Here the accelerance at the midpoint of the beam has been evaluated in the absence and presence of the ATVA. The beam system geometrical and material properties are assumed to be: beam mass, $M_b = 58.8$ kg; beam span, $L_b = 1.5$ m; beam cross-sectional width, $b_b = 0.1$ m; beam cross-sectional thickness, $h_b = 0.05$ m; Young's modulus, $E_b = 200$ GPa; density, $\rho_b = 7850\ \text{kg/m}^3$; and beam loss factor, $\eta_b = 5\%$. For the ATVA system, the mass of the core magnetic circuit, M_s, active mass, M_A, and loss factor are assumed to be 4.0 kg, 2.0 kg and 2%, respectively. The fundamental natural frequency of the host beam is found to be nearly 50 Hz.

Fig. 3 shows the magnitude of the accelerance transfer function of the beam without and with integrated ATVA tuned at the fundamental frequency of the beam (50 Hz). It is noted that stiffness of the ATVA is tuned at $K = \omega_a^2 M_a = (50 \times 2\pi)^2 \times 2 \cong 197$ kN/m to have natural frequency of about 50 Hz. It is also noted that accelerance has been normalized with respect to the reference accelerance defined as $H_r = 1/M_b$ in log scale. As it can be realized, the response of the beam in absence of the ATVA has only

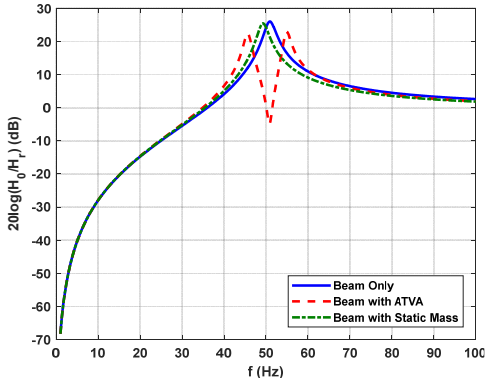

Fig. 3 Accelerance responses versus excitation frequency with respect to first mode function at the midpoint

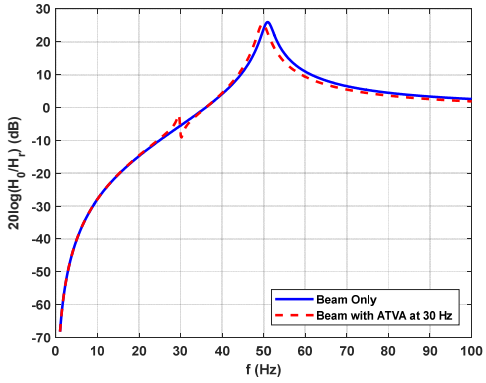

(a)

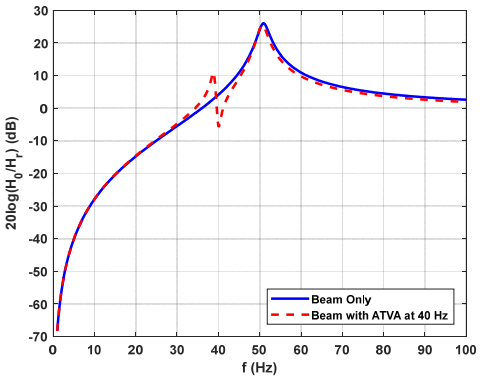

(b)

Fig. 4 Accelerance responses versus excitation frequency with respect to first mode function at the midpoint while the frequency of the ATVA is at (a) 30 Hz; and (b) 40 Hz

one peak which represents the resonance of the beam at its first natural frequency. On the other hand, the accelerance of the beam integrated with ATVA shows drastic reduction in the response at resonance frequency of the host beam at 50 Hz.

In order to investigate the influence of the body mass of ATVA on the response of the system, the accelerance of the beam with and without ATVA is also compared with that of the beam in presence of only static core mass (M_s) of ATVA (H_S) as shown in Fig. 3. As it can be realized from the graphs in this figure, the natural frequency of the system with static core mass slightly decreases compared with that of the bare beam as expected due to increase in the mass of the beam.

Fig. 4 also illustrates the accelerance of the beam where ATVA tuning frequency is set at 30 and 40 Hz, while the natural frequency of the host structure (beam) is around 50 Hz. As it can be seen in these figures, the accelerance response of the beam shows a notch when the excitation frequency is equal to the tuning frequency of the ATVA. In addition, the response of the beam at its natural frequency slightly decreases by integrating it with ATVA tuned at 30 and 40 Hz. However, the reduction in the accelerance of the beam at the natural frequency increases as the tuning frequency of the ATVA gets closer to the natural frequency. Therefore, the best performance will be reached by tuning the ATVA's frequency at the natural frequency of the beam.

3. Development, analysis and optimization of an MRE-based ATVA

Fig. 5 shows the schematic of the proposed MRE-based ATVA which is composed of an oscillator, two MRE specimens operating in shear mode, a steel-based magnetic core, and two coils wound on the core. The frequency shift of the MRE-based ATVA is defined as the difference between its natural frequency when maximum magnetic field is applied to the MRE (ON-state) and its natural frequency in the absence of the magnetic field (OFF-state). The resonance frequency of the MRE-based ATVA can be expressed as

$$f_a = \frac{1}{2\pi}\sqrt{\frac{k_\tau}{M_a}} \tag{23}$$

where M_a is the active mass of the ATVA, and k_τ is the equivalent stiffness of the MRE specimens.

Considering that the MREs operate in shear mode, the equivalent stiffness and damping of the MRE-based ATVA can be defined as

$$\begin{cases} k_\tau = \dfrac{2G'\bar{A}_{MRE}}{h_{MRE}} \\ c_\tau = \dfrac{2G''\bar{A}_{MRE}}{\omega h_{MRE}} \end{cases} \tag{24}$$

where $\bar{A}_{MRE}$ and h_{MRE} are the cross-section area, and thickness of the MREs, respectively. G' and G'' are the storage and loss moduli of the MRE layers operating in shear mode, respectively, which make the complex shear modulus, G, of the MREs as

$$G = G' + iG'' \tag{25}$$

where i represents square root of -1, $i = \sqrt{-1}$.

3.1 Experimental characterization and development of model

MRE sample with 40% volume fraction of iron particles fabricated by CKM Company is utilized to characterize its viscoelastic properties with respect to varied excitation frequency and applied magnetic field. For this purpose, an advanced rotary rheometer equipped with magneto-rheology accessory (DHR-3, TA Instruments) has been utilized (Fig. 6). Oscillation tests have been conducted in linear viscoelastic region at various excitation frequencies under different magnitudes of applied magnetic field and subsequently the storage and loss moduli of the MRE were evaluated experimentally. Finally, a phenomenological material model based on Chebyshev polynomials is proposed to accurately predict the variation of the storage and loss moduli of MREs with respect to the excitation frequency and applied magnetic flux density.

3.1.1 Characterization of MRE

In order to identify the influence of the strain amplitude, excitation frequency, and applied magnetic flux density on the viscoelastic properties of MREs, oscillatory shear tests have been performed on an MRE sample with 40% volume

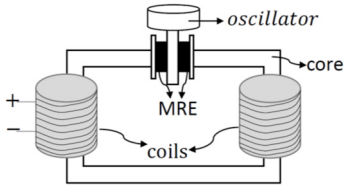

Fig. 5 Schematic of MRE-based ATVA operating in shear mode

Fig. 6 Discovery HR-3 magnetorheological rheometer used for characterization of MRE

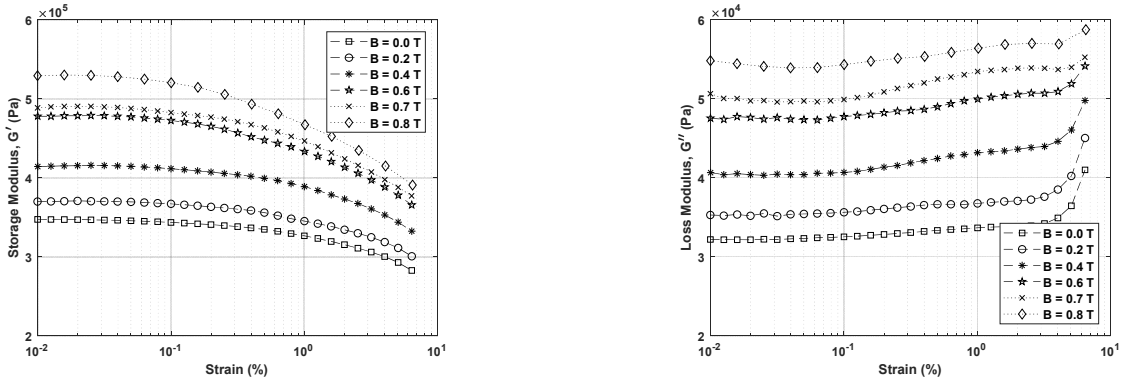

(a) (b)

Fig. 7 Variation of (a) storage and (b) loss moduli with respect to shear strain amplitude for different levels of applied magnetic flux densities

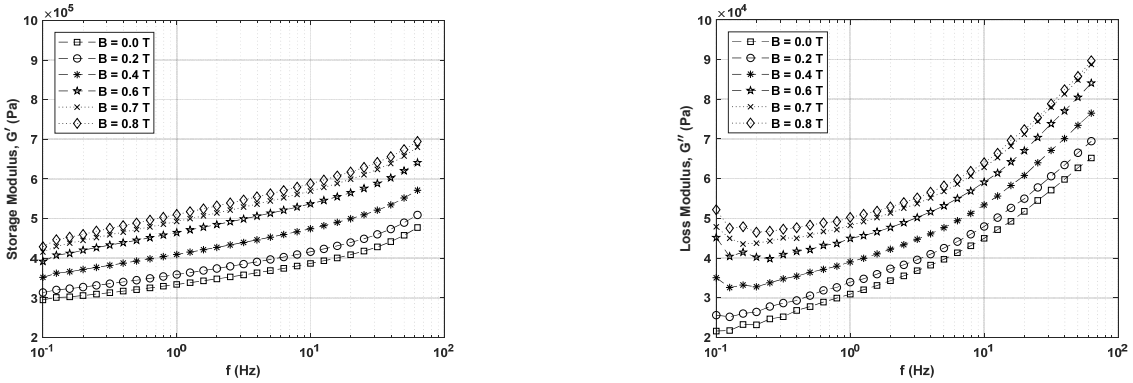

(a) (b)

Fig. 8 Variation of (a) storage, and (b) loss moduli with respect to excitation frequency for different levels of applied magnetic flux densities

fraction of iron particles. For this purpose, an advanced rotary rheometer equipped with magneto-rheology accessory was used (DHR-3, TA Instruments). It should be noted that all the tests were conducted on a sample with 6 mm thickness while pre-loaded under 30 N axial load to prevent slippage. First, the oscillatory test was performed by sweeping the shear strain amplitude from 0.01% to 10% while the excitation frequency was maintained at 1.0 Hz. The test was conducted under various magnitudes of applied magnetic field (0.2, 0.4, 0.6, 0.7, and 0.8 T) and at room temperature (20℃).

Fig. 7 shows the variation of the storage and loss moduli with respect to the strain amplitude for various levels of applied magnetic flux density. As it can be realized, the storage modulus is almost independent of the strain amplitude for the strain amplitudes up to 0.1%, so called linear viscoelastic region. However, the MRE operates in nonlinear viscoelastic region by further increasing the strain amplitude in which storage modulus decreases drastically. Moreover, results show that both storage and loss moduli increase by enhancing the applied magnetic flux density. This relationship demonstrates field stiffening effect of MREs which could potentially exploited for vibration control applications.

Since the aim is to operate in linear viscoelastic region, the next round of tests was conducted to investigate the influence of excitation frequency on the storage and loss moduli of the MRE while limiting strain amplitude to under 0.1%. For this purpose, the oscillation shear tests were conducted at the strain amplitude of 0.01% (linear viscoelastic region) while the excitation frequency were swept from 0.1 to 70 Hz. Fig. 8 shows the variation of the storage and loss moduli with respect to the excitation frequency for various levels of applied magnetic flux density. The results clearly show that storage and loss moduli increase with increasing the excitation frequency.

Fig. 9 shows the change of the storage and loss moduli due to the applied magnetic flux density ($\Delta G'$ and $\Delta G''$) for various excitation frequencies. As it can be realized, the change in both moduli due to the applied magnetic field enhances with increasing the intensity of magnetic field. Moreover, the effect of magnetic field on the change in storage modulus increases by increasing the excitation frequency and $\Delta G'$ is noticeably higher for 50 Hz compared with that in 0.1 Hz. Moreover, results show that the increment of storage modulus ($\Delta G'$) is larger than that of loss modulus ($\Delta G''$) under the same condition.

Table 1 Identified parameters for the storage and loss moduli of MRE in Pa as a function of applied magnetic flux density in T and excitation frequency in Hz

	α_{11}	α_{12}	α_{13}	α_{21}	α_{22}	α_{23}	α_{31}	α_{32}	α_{33}
$G'(B,\omega)$	389461.6	179316	42333	2924.551	1292.611	159.0622	-6.45796	-5.71708	-0.55291
$G''(B,\omega)$	38893.98	16682.03	4698.478	875.1306	231.4784	-43.3019	-3.30609	-0.38855	0.135638

3.1.2 Development of a material model for the MRE

Considering experimental observation in Section 3.1.1, linear viscoelastic properties of MREs highly depends on the input excitation frequency and applied magnetic flux density. Thus, development of a material model which can accurately predict the variation in storage and loss moduli under any excitation and magnetic flux density is of paramount importance for the development of the mathematical model for MRE-based ATVAs. In the present study, a parametric model based on Chebyshev polynomials is proposed to describe the shear moduli as a function of both applied magnetic flux density and excitation frequency. Chebyshev polynomials are a sequence of orthogonal polynomials which can be defined recursively. They are important in approximation theory in mathematics. Predominantly, Chebyshev polynomials have two kinds of forms. The roots of the Chebyshev polynomials of the first kind, which are also called Chebyshev nodes, are generally used as nodes in polynomial interpolation. The corresponding polynomial interpolation can minimize the problem of the Runge's phenomenon (Nocedal and Wright 1999) and can provide a best approximation of the given continuous function. The polynomials of the first and second kinds are basically the solution to the Chebyshev differential equations, which are

$$(1-x^2)y'' - xy' + n^2 y = 0 \tag{26}$$

and

$$(1-x^2)y'' - 3xy' + n(n+2)y = 0 \tag{27}$$

respectively.

The Chebyshev polynomials of the first kind are used in this research study, which are defined by the recurrence relation as

$$\begin{cases} T_0(x) = 1 \\ T_1(x) = x \\ T_{n+1}(x) = 2xT_n(x) - T_{n-1}(x) \end{cases} \tag{28}$$

As discussed before, in the linear viscoelastic region, the shear storage and loss moduli are independent of strain amplitude, however they depend on both magnetic flux density and excitation frequency. Thus, the following frequency and magnetic field dependent parametric model utilizing the first-kind Chebyshev polynomials is proposed

$$G = (a_1 F_1 + a_2 F_2 + a_3 F_3)(c_1 B_1 + c_2 B_2 + c_3 B_3) \tag{29}$$

where a_n and c_n $(n = 1, 2, 3)$ are coefficients of the polynomials function. F_n and B_n $(n = 1, 2, 3)$ are the first three polynomials of first kind Chebyshev polynomials with respect to frequency and magnetic flux density, respectively. Expanding Eq. (29) and combing the multiplied coefficients (a_n and c_n) into new coefficients (α_{nn}), we can write

$$\begin{aligned} G' \text{or } G''(B,\omega) = {} & \alpha_{11}F_1B_1 + \alpha_{12}F_1B_2 + \alpha_{13}F_1B_3 \\ & + \alpha_{21}F_2B_1 + \alpha_{22}F_2B_2 + \alpha_{23}F_2B_3 \\ & + \alpha_{31}F_3B_1 + \alpha_{32}F_3B_2 + \alpha_{33}F_3B_3 \end{aligned} \tag{30}$$

Least square minimization technique in MATLAB optimization toolbox has been utilized to identify the coefficients to minimize the error between the model and the experimental results. Table 1 presents the coefficient of the Chebyshev polynomials for both storage and loss moduli of the MRE.

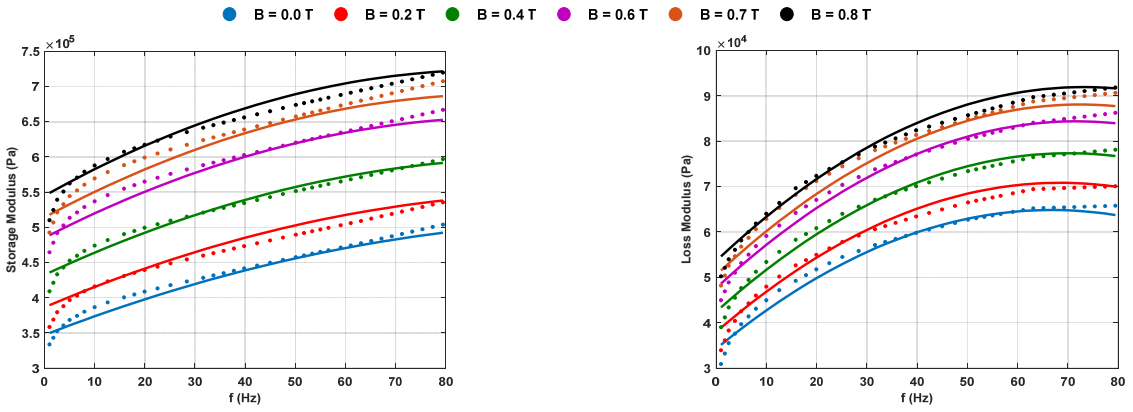

(a) (b)

Fig. 10 The results of the (a) storage and (b) loss moduli with respect to frequency. Experiment data "." Fitting results "-"

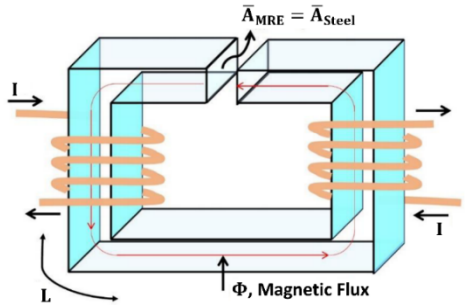

Fig. 11 Schematic of a C-shape electromagnet

Fig. 10 shows the experimental results and those predicted using the proposed model for storage and loss moduli with respect to excitation frequency for various levels of applied magnetic flux density. As it can be realized, experimental results and those predicted using the model are correlated well especially for magnetic flux densities below 0.7 T. The MRE is magnetically saturated by increasing the applied magnetic flux density above 0.7 T, which results in higher discrepancies between the experimental and model results. The accuracy of the developed approximate analytical model is also examined quantitatively using R^2 (R-Squared) known as the coefficient of determination. This is basically a statistical measure which demonstrates the accuracy of the developed regression model to fit the experimental data. The R^2 ranges between 0 and 100% in which 100% represents that the model perfectly represents the experimental data and its variability around the mean value over the whole design space. Here it is found that R^2 is over 95% for all cases demonstrating that the Chebyshev polynomial-based model can accurately describe the variation of the moduli with respect to both frequency and magnetic flux intensity.

3.2 Design of electromagnet and magnetic circuit

Fig. 11 shows a schematic of electromagnet utilized in the design of the proposed ATVA. When the electric current is supplied to the coils, the generated magnetic flux is guided through the electromagnet C-shape core frame and passes through MRE specimen which is placed in the gap as shown in Fig. 11. Considering Figs. 5 and 11, the MREs are under shear motion which is perpendicular to the magnetic flux line passing through the MREs. Thus, through the application of the magnetic field, the shear modulus of MREs can be instantly and reversibly changed and thus the natural frequency of the absorber can be adaptively altered by controlling the supplied current to the electromagnet.

One of the main objectives of the present study is to design a MRE-based ATVA to have minimum weight and maximum dynamic range, which is defined as the ratio of the natural frequency of the ATVA in ON-state to that of OFF-state, while satisfying the geometrical and magnetic circuit requirements.

An ideal magnetic circuit aims at providing a low reluctance flux conduit to guide and concentrate magnetic flux into the region where MRE resides and maximizing the magnetic field energy in the MRE. Moreover, the magnetic circuit is required to maintain sufficient cross section of steel core to keep the magnetic field intensity, H, in the steel very low while minimizing the energy lost in the underutilized areas and the weight of the core steel.

Typically, the procedure of designing magnetic circuit in MR based devices consists of the following steps (Lord M Solutions 2001):

STEP #1: Select required operating point magnetic flux density, B_{MRE}, in the given B-H curve of MRE. It is noted that the magnetic flux in the MRE specimen can be obtained as: $\Phi_{MRE} = B_{MRE} \times \bar{A}_{MRE}$ in which B_{MRE} is the required magnetic flux density in the MRE and $\bar{A}_{MRE}$ is the cross-sectional area of the MRE.

STEP #2: Evaluate the magnetic flux density in the steel core conduit by applying the conservation of the magnetic flux density in the magnetic circuit as

$$\Phi_{MRE} = \Phi_{Steel} = B_{MRE}\,\bar{A}_{MRE} = B_{Steel}\,\bar{A}_{Steel}$$
$$\Rightarrow B_{Steel} = \frac{\Phi_{Steel}}{\bar{A}_{Steel}} = \frac{B_{MRE}\bar{A}_{MRE}}{\bar{A}_{Steel}} \quad (31)$$

STEP #3: Determine the magnetic field intensity in the steel core, H_{Steel}, using evaluated B_{Steel} in Step # 2 and available B-H curve for steel.

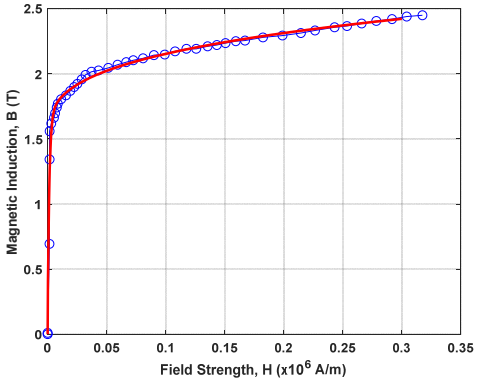

(a)

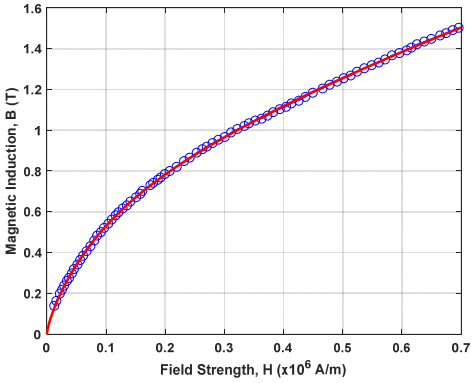

(b)

Fig. 12 Magnetic induction versus field strength of (a) steel and (b) 40% isotropic MRE Extract points "o" and model results "-"

Table 2 Identified parameters for B-H relations

Material	Function of B versus H curve	R^2
1117 steel	$B = 1.44(1-e^{-731.1H}) + 1.3843H^{0.29}$	0.97
40% isotropic MRE	$B = 0.2457(1-e^{-12.615H}) + 1.5870H^{0.6506}$	0.99

STEP #4: Evaluate the required amp-turns utilizing the Ampere's law as

$$\oint \mathrm{hdl} = \mathrm{NI} \implies H_{MRE} \times 2h_{MRE} + H_{Steel} \times L = NI \quad (32)$$

where h_{MRE} is the thickness of the MRE specimen, L is the total length of the flux going through the C-shape steel conduit, N is the total turns of coils in the circuit, I is the input current, H_{MRE} is the magnetic field in MREs and H_{Steel} is the magnetic field in the steel which is considered to be AISI 1117 carbon steel.

As explained above to design magnetic circuit it is essential to have B-H curves for both MRE and steel materials. For this purpose, the magnetic flux density versus magnetic strength curves for AISI 1117 steel and MRE with 40% volume fraction of iron particles are presented in Fig. 12. Based on the exponential trend and saturation phenomenon in B-H curve, here a model is proposed to predict the induced magnetic flux density in MRE and steel for the given magnetic field intensity as

$$B = a_B \times \left(1 - e^{-b_B \times H}\right) + c_B \times H^{d_B} \quad (33)$$

where B denotes magnetic flux density in T, and H is magnetic field intensity in MA/m. Constant parameters a_B, b_B, c_B, d_B are unknown coefficients of the function which have been identified using least square minimization technique in the MATLAB optimization toolbox to minimize the error between estimated and experimental data. Table 2 provides the proposed functions for steel and MRE together with the R^2 values. Fig. 12 also shows the predicted B-H curves for MRE and steel using the proposed relations and their comparison with real experimental data. As it can be realized the proposed B-H relations can accurately characterize and capture the magnetic properties of MREs and steel.

3.3 Multidisciplinary design optimization formulation

For the proposed MRE based ATVA design shown in Fig. 5, the geometrical and magnetic circuit parameters as well as the mass of oscillator, M_a, have been considered as potential design variables which affect the ATVA's resonance frequency. As shown in Fig. 13, the ATVA consists of two coils winding on each side of the core with vertical and horizontal number of coils of N_a and N_b, respectively, two MRE specimens with thickness and side length of h_{MRE} and a, respectively, located in the gap between the core frame and oscillator mass and finally active mass of M_a. Therefore, the following design variable vector which will be utilized later for design optimization problem has been identified

$$X = \{a, h_{MRE}, N_a, N_b, M_a\} \quad (34)$$

Using Eqs. (23) and (24), the change in the natural frequency due to the application of the maximum flux density of B = 0.8 T (which is prescribed by maximum current 2.0 A) can be expressed as

$$\delta f_a = \frac{1}{2\pi}\left(\sqrt{\frac{2G'_{max}\, a^2}{M_a\, h_{MRE}}} - \sqrt{\frac{2G'_{min}\, a^2}{M_a\, h_{MRE}}}\right) \quad (35)$$

in which G'_{max} is maximum storage modulus induced in the MRE due to the application of maximum current while G'_{min} is the minimum storage modulus of MRE in the absence of the applied magnetic field. It is noted that the MRE covers the whole cross-sectional area of the steel core, thus $\bar{A}_{MRE} = a^2$. A multidisciplinary design optimization problem accounting for both the geometry and magnetic circuit parameters is formally formulated to maximize the frequency range of the proposed MRE-based ATVA while minimizing its mass as:

Find design variable vector $X = \{a, h_{MRE}, N_a, N_b, M_a\}$

To

$$\text{Minimize} \quad \text{Obj\_Func} = (M_s + M_a) - (\delta f_a) \quad (36)$$

Subject to constraints

$$\begin{aligned}
&g_1: \text{Side length of MRE:} \quad 20 \le a \le 50 \text{ mm}\\
&g_2: \text{Thickness of MRE:} \quad 1 \le h_{MRE} \le 8 \text{ mm}\\
&g_3: \text{Vertical turns of each coil:} \quad 10 \le N_a \le 100\\
&g_4: \text{Horizon turns of each coil:} \quad 10 \le N_b \le 100\\
&g_5: \text{Mass of the oscilliator:} \quad 0.1 \le M_a \le 2 \text{ Kg}\\
&g_6: \text{Total mass of the ATVA:}\\
&\quad 0.1 \le M_s + M_a \le 5 \text{ Kg}\\
&g_7: \text{Frequency at zero current:}\\
&\quad f_a(I=0) = f_{a_{min}} \le f_{beam}\\
&g_8: \text{Frequency at maximum current:}\\
&\quad f_{beam} \le f_a(I=2) = f_{a_{max}}\\
&g_9: \text{Length of the flux in the core:}\\
&\quad L = \frac{NI - 2\, h_{MRE}\, H_{MRE}}{H_{Steel}}\\
&\quad \ge 2\, L_a + 2\, L_b - 2\, h_{MRE} - t_s
\end{aligned} \quad (37)$$

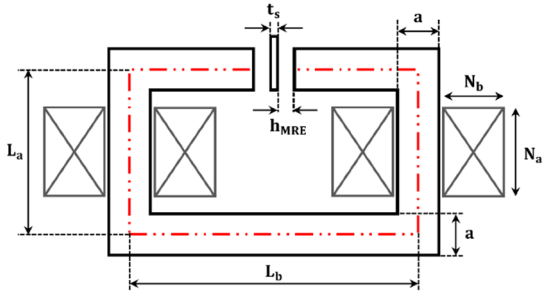

Fig. 13 The sectional magnetic coils and core of the MRE-based ATVA

where the total mass of the ATVA excluding the active mass (M_a) can be obtained as

$$M_s = M_{core} + 2M_{coil} \tag{38}$$

Where

$$\begin{cases} M_{core} = La^2\rho_{Steel} \\ M_{coil} = [(2N_b d_w + a)^2 - a^2]N_a d_w \rho_{Copper} \end{cases} \tag{39}$$

Moreover, due to the geometrical restriction of the magnetic circuit as shown in Fig. 12, we should have

$$\begin{aligned} g_{10}&: \quad L_a \geq N_a\, d_w + a \\ g_{11}&: \quad L_b \geq 2N_b\, d_w + a + 2h_{MRE} + t_s \end{aligned} \tag{40}$$

It is noted that in the above relations

$$\begin{cases} G'_{max} = G'_0 + \Delta G_d \\ G'_{min} = G'_0 \\ 0 \leq w_1 \leq 1 \\ 0 \leq w_2 \leq 1 \\ I_{max} = 2.0\ A \\ B_{max} = 0.8\ T \\ f_{beam} = 50\ Hz \end{cases} \tag{41}$$

It is also noted that the constraint on the flux length in the C-shaped core given in Eq. (37) has been derived using the Ampere's law for the magnetic circuit as

$$NI = 2h_{MRE}\, H_{MRE} + L\, H_{Steel} \tag{42}$$

Also, using Fig. 13, the total flux length, L, can be described as

$$L \geq 2L_a + 2L_b - 2h_{MRE} - t_s \tag{43}$$

Thus, using Eqs. (42) and (43), we can write

$$\frac{NI - 2h_{MRE}\, H_{MRE}}{H_{Steel}} \geq 2\, L_a + 2\, L_b - 2\, h_{MRE} - t_s \tag{44}$$

The total turns of wires in the ATVA has also been approximated as

$$N = 2\, N_a\, N_b \tag{45}$$

It is noted in the constraint relation in Eq. (37), the term f_{beam} is the first natural frequency of the host simply supported beam and $f_{a_{min}}$ is the OFF-state natural frequency of the MRE absorber. The purpose is to ensure that absorber resonance frequency in the absence of the magnetic field is lower than the fundamental frequency of the host beam which is found previously to be at 50 Hz. The maximum current I are fixed at $I_{max} = 2.0\ A$ due to practical limitations such as safety and heat generation issues. The magnetic circuit is designed in a way to have $B_{max} = 0.8\ T$, which is saturation point of the characterized MRE samples with 40% volume fraction of iron particles at 2.0 A. ρ_{Steel} is the density of the steel given as 7.90 g/cm^3 and ρ_{Copper} is the density of the copper, 8.92 g/cm^3. G'_{min} is the shear modulus of the MRE when $I = 0\ A$, while G'_{max} is the storage modulus when $I = 2.0\ A$. t_s is the width of the massless rigid plate bounded to MRE specimens to rigidly transfer motion to the isolator active mass and is set at $t_s = 5.0\ mm$, d_w is the diameter of the AWG18 wire used for the magnetic coils which is $d_w = 1.0\ mm$.

3.3.1 Optimization results

The sequential quadratic programming (SQP) algorithm, which is a powerful non-linear gradient based optimization algorithm, has been utilized in this study to solve the formulated optimization problem defined in Section 3.3. The SQP algorithm is based on iterative quadric approximation of the Lagrangian at each optimization iteration. In this study, a program in MATLAB environment has been written to execute and solve the formulated optimization problem in Eqs. (36), (37) and (39) using SQP algorithm. It is noted that SQP algorithm is a local optimizer without any mechanism to search for global optimum solution. Considering this, numerous random initial points have been used to assure that the global optimum solution has been captured. Several of these initial points are provided in Table 3.

Optimal results are provided in Table 4. As it can be realized SQP optimizer has led to same optimal design variables starting from diffident intimal points. It should be noted that the constraints on side length (g_1) and N_b (g_4) in constraint relations in Eq. (37) are active ($a = 20\ mm$ and $N_b = 10$). Additional constraints on length L_a and L_b provided in Eq. (39) (g_{10} and g_{11}) are also active. For this case, the optimal total mass of the MRE-based ATVA is found to be almost 2.50 kg with active mass of only 1.07 kg resulting in an ATVA's frequency range of about 11.4 Hz. This represents 23% change in ATVA frequency which is remarkable considering ATVA's total mass of only 2.5 kg. It is noted that the total mass of the host beam is 58.8 kg, thus the total mass of the absorber is only about 2.5/58.9 = 4.2% of the total mass of the beam which is very ideal (in practical application mass of a TVA should be less than 10% of the total mass of the host structure). Optimization results for vertical and horizontal wire turns are also found to be 40 and 10, respectively resulting in total $2 \times 40 \times 10 = 800$ turns of wire in the magnetic circuit. The optimization has also resulted in optimal MRE thickness of 3.5 mm within the allocated range.

Table 3 Initial points for the multidisciplinary design optimization problem

	a (mm)	$\mathbf{h_{MRE}}$ (mm)	$\mathbf{N_a}$	$\mathbf{N_b}$	$\mathbf{M_a}$ (Kg)
Case (a)	20	1.0	10	10	0.5
Case (b)	30	4.0	30	30	1.0
Case (c)	40	6.0	60	60	1.0
Case (d)	50	8.0	80	80	1.5

Table 4 Optimal results of the multidisciplinary design optimization problem

	a (mm)	h_{MRE} (mm)	N_a	N_b	L_a (mm)	L_b (mm)	M_a (kg)	M_s (kg)	M_t (kg)	$f_{a_{min}}$ (Hz)	$f_{a_{max}}$ (Hz)	δf_a (Hz)
Cases (a)-(d)	20	3.5	40	10	60	52	1.07	1.43	2.50	49.7	61.1	11.4

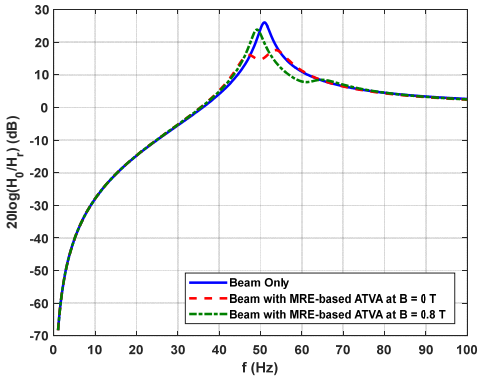

Fig. 14 Performance of the optimized ATVA in absence and presence of magnetic field

Fig. 14 shows the accelerance response of the beam integrated with optimized MRE-based ATVA in absence and presence of the magnetic field. It is noted that the stiffness and damping of the ATVA is obtained using Eq. (24) and developed models for G' and G'' in Eq. (30). Results show that increasing the applied magnetic flux density from 0 to 0.8 T rises the natural frequency of the MRE-based ATVA (anti-resonance in integrated beam and ATVA system) from 49.7 Hz to 61.1 Hz which shows the adaptability of the designed light-weight ATVA (total mass of only 2.5 kg) to suppress vibration of the host beam around its fundamental frequency of 50 Hz due to change in excitation conditions.

4. Development of a tuning controller for the optimal MRE-based ATVA

As it was mentioned before, MRE-based ATVA's performance in attenuating the vibration of a host system depends on its ability to tune its natural frequency and track the excitation frequency accordingly. For this purpose, the excitation frequency is required to be identified in real-time. As direct measurement of excitation frequency is not possible, it is generally attempted to indirectly track the excitation frequency through measurement of system responses such as displacement, velocity or acceleration using appropriate sensors. Acceleration is usually preferable as it can be easily and accurately measured experimentally using accelerometers. Looking into the vibration response of the absorber and the host system, it can be realized that the excitation frequency is mainly related to the phase difference (α) between the harmonic response of the oscillator active mass and the host system (Liao *et al*. 2013, Rasooli *et al*. 2020). Fig. 15 shows the schematic of the equivalent two degrees of freedom (DOF) system representing the beam and integrated MRE-based ATVA shown in Fig. 2. As it can be seen, the beam and the static

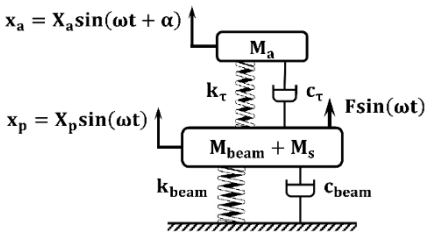

Fig. 15 Schematic of the equivalent system integrated with MRE-based ATVA

mass of the absorber are considered as a lumped mass in the equivalent system which is connected to the absorber's resonator mass (M_a) using equivalent stiffness and damping (k_τ and c_τ) of the MRE. It should be noted that the equivalent stiffness and damping of the host at the mid-point and associated with the fundamental mode are $\frac{\pi^4 E_b I_b}{L_b^3}$ and $\frac{\pi^4 E_b I_b \eta_b}{L_b^3 \omega}$, respectively.

The governing equations of motion of the two-DOF system can be easily derived using 2nd law of Newton from which, the phase difference (φ) between the absolute acceleration of the host structure ($\ddot{x}_p$) and the relative acceleration of the host and the adaptive absorber's resonator ($\ddot{x}_a - \ddot{x}_p$) may be described as

$$\varphi = \begin{cases} \tan^{-1}\dfrac{2\xi_a \Omega}{\Omega^2 - 1} & \Omega > 1 \\ \dfrac{\pi}{2} & \Omega = 1 \\ \tan^{-1}\dfrac{2\xi_a \Omega}{\Omega^2 - 1} + \pi & \Omega < 1 \end{cases} \tag{46}$$

where Ω is the ratio of the natural frequency of the absorber to the excitation frequency ($\Omega = \frac{\omega_a}{\omega} = \frac{f_a}{f}$) and ξ_a is the damping ratio of the absorber ($\xi_a = \frac{c_\tau}{2M_a\omega_a}$). Fig. 16 shows the variation of the phase difference with respect to the frequency for the system integrated with optimum MRE-based ATVA tuned to operate in the absence of magnetic field ($f_a = f_{a_{min}} = 49.7$ Hz), and in presence of maximum magnetic flux density of 0.8 T ($f_a = f_{a_{max}} = 61.1$ Hz), and at the natural frequency of the beam ($f_a = f_{beam} = 50$ Hz). Results suggest that regardless of the tuning frequency of the ATVA, the phase difference is less than 90° for the excitation frequencies less than the tuning frequency of the ATVA and passes 90° as the excitation frequency goes above the tuning frequency. Therefore, identifying the phase difference between the relative acceleration and absolute acceleration of the host system provides the opportunity to determine whether the tuning frequency needs to be increased or decreased in order to

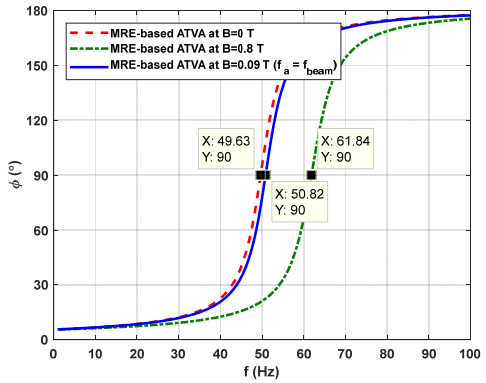

Fig. 16 Phase difference between the relative acceleration of the host system and ATVA's resonator and the absolute acceleration of the host

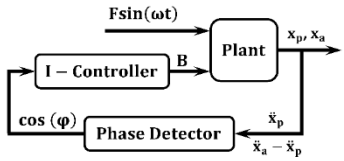

Fig. 17 Schematic of the tuning controller for MRE-based ATVA

track the excitation frequency.

Phase angle can be practically measured through measurement of absolute acceleration of the host structure and the relative acceleration of the host and the adaptive absorber. It can be shown that the multiplication of two harmonic signals with amplitudes of X_p and X_{a-p} and frequency and phase difference of ω and φ, respectively, results in a constant part, $2X_pX_{a-p}\cos(\varphi)$, and a harmonic part, $2X_pX_{a-p}\cos(2\omega t-\varphi)$. Similarly, square of each of the signals results in constant and harmonic parts as $\frac{X_{p,a-p}^2}{2}$ and $\frac{X_{p,a-p}^2}{2}\cos(2\omega t+2\varphi)$, respectively. Using a low pass filter the harmonic part of each of results can be filtered to obtain the cosine of the phase difference, $\cos(\varphi)$ as well as the amplitude of each signal (Liao *et al*. 2013, Rasooli *et al*. 2020). Considering the phase angle presented in Eq. (45) and Fig. 16, it is clear that the cosine of φ is positive when the excitation frequency is less than tuning frequency of the ATVA (f_a) and it is negative for the case that excitation frequency is higher than f_a. Therefore, a simple control law for tuning the MRE-based ATVA may be defined as

$$\frac{dB}{dt}=\gamma\cos(\varphi) \tag{47}$$

where γ is a negative gain. Fig. 17 shows the schematic of the tuning control algorithm for the MRE-based ATVA. As it can be seen, the measured relative and absolute accelerations are sent to the phase detector to evaluate the phase difference as $\cos(\varphi)$. Then the required magnetic flux density (B) is calculated using a I-controller which will vary accordingly the stiffness and damping of the MRE-based ATVA to change its natural frequency and track the excitation frequency.

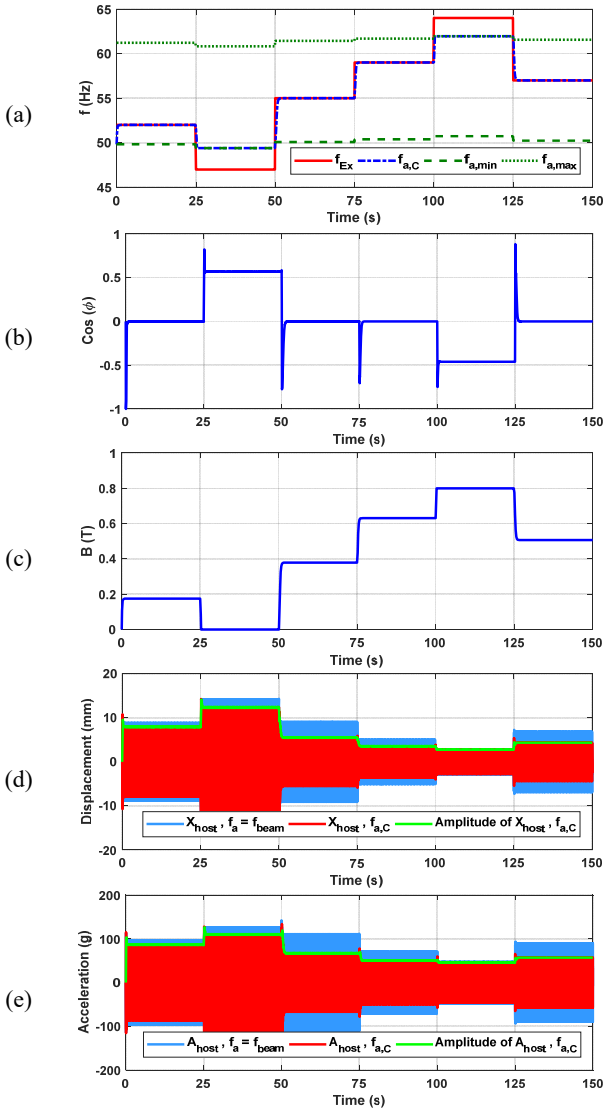

Fig. 18 Simulation results of (a) natural frequency of MRE-based ATVA; (b) cosine of phase difference; (c) applied magnetic flux density; (d) displacement of the host; (e) acceleration of the host

The tuning control algorithm is simulated in MATLAB-Simulink to evaluate its capability in identifying the phase difference and tracking the excitation frequency. Figs. 18(a) to (e) show the time responses of changes in the ATVA's natural frequency, identified $\cos(\varphi)$, applied magnetic flux density and displacement and acceleration of the host system, respectively. As it can be seen in Fig. 18(a), the excitation frequency has been changed every 25 s starting with the initial excitation frequency of 52 Hz. Results show that the controller swiftly responded to the detected phase difference and changes the applied magnetic field to set the natural frequency of the absorber (f_{a_C}) equal to the excitation frequency, set at 55, 59 and 57 Hz in the time intervals of 50-75, 75-100 and 125-150 s. During these periods, the controller enhances the magnetic flux density to 0.38, 0.63, and 0.51 T (by adjusting the current to the electromagnet) to tune the ATVA's operating frequency at 55, 59, and 57 Hz, respectively.

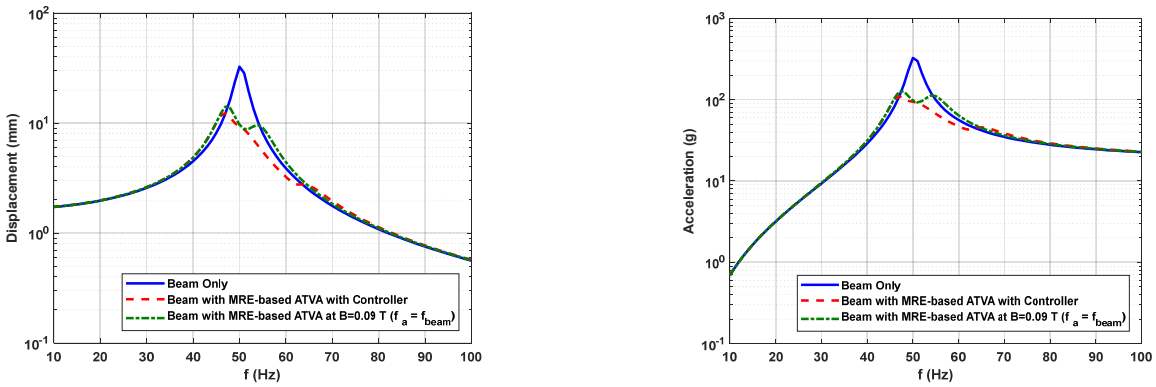

(a) (b)

Fig. 19 (a) Displacement; and (b) acceleration of the beam in absence of MRE-based ATVA and in presence of MRE-based ATVA (with controller and tuned at natural frequency of the beam)

However, the controller could not track the excitation frequency during time periods of 25-50 and 100-125 s when the excitation frequency is set at values which are lower than the minimum, (49.4 Hz), and higher than maximum, (61.95 Hz), natural frequency of the absorber. This is also clear from Fig. 18(b) in which the cosine of phase angle is not zero during these two periods. Fig. 18(c) also shows that the applied magnetic flux density is set at 0 and 0.8 T by the controller during 25-50 and 100-125 s time intervals, respectively, which are the lower and upper limits for the designed MRE-based ATVA. It should be mentioned that choosing the gain of the I-controller (γ) as -1 results in maximum settling time of 1.5 s which indicates an instantaneous response of the controller. Figs. 18(d) and (e) present the displacement and acceleration of the host, respectively, for the case that the natural frequency of the MRE-based ATVA is tuned at the natural frequency of the beam ($B = 0.09$ T) and the case of controlled MRE-based ATVA. As it can be seen in these figures, adaptive tuning of the operating frequency of the absorber significantly increases its performance in attenuating the displacement and acceleration of the host through the frequency range of interest.

As mentioned before, the amplitude of a harmonic signal can be identified by passing the square of the signal through a low pass filter. The green line in Figs. 18(d) and (e) show the identified amplitude of the displacement (X_p) and acceleration ($\ddot{X}_p$) of the host for the case of controlled MRE-based ATVA. Results show that the filter could successfully extract the amplitude in real time. Results also confirm that for each 25 s time interval the transient part of the responses are very limited, less than 2.0 s, and the responses quickly approach to the steady state condition. Fig. 19 presents the steady state response of the displacement and acceleration of host with respect to frequency in which the frequency responses of the beam without ATVA, beam integrated with passive MRE-based ATVA tuned at its natural frequency ($f_a = f_{beam}$), and beam with controlled MRE-based ATVA are presented. The superior performance of the controlled MRE-based ATVA compared to the passive TVA is clear in this figure.

5. Conclusions

The present study developed a multidisciplinary design optimization framework to improve the performance of MRE-based ATVA for an elastic beam. The accelerance transfer function of the host beam has been derived and analyzed to evaluate the performance of the ATVA. Experiments on 40% volume fraction of isotropic MRE have been conducted and results have been analyzed. Utilizing the experimental data, the Chebyshev Polynomials are utilized to describe the dynamic behavior of the MREs in terms of magnetic flux density and excitation frequency. Moreover, using the Ampere's law for the magnetic circuit an analytical equation has been derived to relate the geometrical and magnetic circuit parameters. Subsequently, formal multi-objective multidisciplinary design optimization problem has been formulated to identify the optimal parameters of the proposed design to maximize the frequency bandwidth of the proposed MRE-based ATVA while limiting its mass. A maximum frequency range of 11.4 Hz which is equivalent to 23% of the beam's resonance frequency (50 Hz) has been achieved with ATVA's total mass of only 2.5 kg which constitutes 4.2% of the total mass of the host simply supported beam. Finally, a tuning algorithm has been presented to determine the required magnetic flux density in order to tune the resonance frequency of the MRE-based ATVA with the excitation frequency. Evaluating the performance of the controller in both time and frequency domains showed a significant effect of the developed MRE-based ATVA in attenuating the vibration of the beam.

Acknowledgments

This research in part was supported by the Canadian Natural Science and Engineering Research Council (NSERC) under Discovery Grant RGPIN-2017-06764.

References

Ahamed, R., Choi, S.B. and Ferdaus, M.M. (2018), "A state of art on magneto-rheological materials and their potential applications", *J. Intell. Mater. Syst. Struct.*, **29**(10), 2051-2095. https://doi.org/10.1177/1045389X18754350

Deng, H. and Gong, X. (2008), "Application of magnetorheological elastomer to vibration absorber", *Commun. Nonlinear Sci. Numer. Simul.*, **13**, 1938-1947. https://doi.org/10.1016/j.cnsns.2007.03.024

Deng, H., Gong, X. and Wang, L. (2006), "Development of an adaptive tuned vibration absorber with magnetorheological elastomer", *Smart Mater. Struct.*, **15**(5), 111-116. https://doi.org/10.1088/0964-1726/15/5/N02

Gao, P., Xiang, C., Liu, H., Walker, P. and Zhou, H. (2019), "Vibration reduction performance parameters matching for adaptive tunable vibration absorber", *J. Intell. Mater. Syst. Struct.*, **30**(2), 198-212. https://doi.org/10.1177/1045389X18810808

Ginder, J.M., Schlotter, W.F. and Nichols, M.E. (2001), "Magnetorheological elastomers in tunable vibration absorbers", In: *Smart Structures and Materials 2001*: *Damping and Isolation*, Vol. 4331, pp. 103-110.

Ginder, J.M., Clark, S.M., Schlotter, W.F. and Nichols, M.E. (2002), "Magneto-strictive phenomena in magnetorheological elastomers", *Int. J. Modern Phys. B*, **16**(17-18), 2412-2418. https://doi.org/10.1142/S021797920201244X

Hemmatian, M. and Sedaghati, R. (2016), "Investigation on the effect of MR elastomer based adaptive vibration absorbers on the radiated sound from circular elastic plates", In: *Active and Passive Smart Structures and Integrated Systems 2016*, Vol. 9799, p. 97992R.

Hoang, N., Zhang, N. and Du, H. (2009), "A dynamic absorber with a soft magnetorheological elastomer for powertrain vibration suppression", *Smart Mater. Struct.*, **18**(7), 074009. https://doi.org/10.1088/0964-1726/18/7/074009

Hwang, Y., Lee, C.W., Lee, J. and Jung, H.J. (2020), "Feasibility of a new hybrid base isolation system consisting of MR elastomer and roller bearing", *Smart Struct. Syst., Int. J.*, **25**(3), 323-335. https://doi.org/10.12989/sss.2020.25.3.323

Lerner, A.A. and Cunefare, K.A. (2008), "Performance of MRE-based vibration absorbers", *J. Intell. Mater. Syst. Struct.*, **19**(5), 551-563. https://doi.org/10.1177/1045389X07077850

Liao, G., Gong, X. and Xuan, S. (2013), "Phase based stiffness tuning algorithm for a magnetorheological elastomer dynamic vibration absorber", *Smart Mater. Struct.*, **23**(1), p. 015016. https://doi.org/10.1088/0964-1726/23/1/015016

Lin, F. (2019), "Design and optimization of magnetorheological elastomer based adaptive tuned vibration absorber", Master Dissertation; Concordia University, Montreal, Canada.

Liu, G., Lu, K., Zou, D., Xie, Z., Rao, Z. and Ta, N. (2017), "Development of a semi-active dynamic vibration absorber for longitudinal vibration of propulsion shaft system based on magnetorheological elastomer", *Smart Mater. Struct.*, **26**(7), p. 075009. https://doi.org/10.1088/1361-665X/aa73f3

Lord MR Solutions (2001), Magnetic circuit design, Engineering notes.

Nocedal, J. and Wright, S.J. (1999), *Numerical Optimization*, Springer series in operations research.

Popp, K.M., Kröger, M., Li, W.H., Zhang, X.Z. and Kosasih, P.B. (2009), "MRE properties under shear and squeeze modes and applications", *J. Intell. Mater. Syst. Struct.*, **21**(15), 1471-1477. https://doi.org/10.1177/1045389X09355666

Qian, L.J., Xin, F.L., Bai, X.X. and Wereley, N.M. (2017), "State observation–based control algorithm for dynamic vibration absorbing systems featuring magnetorheological elastomers: Principle and analysis", *J. Intell. Mater. Syst. Struct.*, **28**(18), 2539-2556. https://doi.org/10.1177/1045389X17692047

Rasooli, A., Hemmatian, M. and Sedaghati, R. (2020), "Phase based control of a novel beam-shape MRE-based adaptive tuned vibration absorber", In: *AIAA Scitech 2020 Forum*, p. 1768.

Skalski, P. and Kalita, K. (2017), "Role of magnetorheological fluids and elastomers in today's world", *Acta Mechanica et Automatica*, **11**(4), 267-274. https://doi.org/10.1515 / ama-2017-0041

Thomson, W.T. and Dahleh, M.D. (1998), *Theory of Vibration with Applications*, (5th Edition), Prentice Hall.

Zhang, X.Z. and Li, W.H. (2009), "Adaptive tuned dynamic vibration absorbers working with MR elastomers", *Smart Struct. Syst., Int. J.*, **5**(5), 517-529. https://doi.org/10.12989/sss.2009.5.5.517

Zhang, X., Peng, S., Wen, W. and Li, W. (2008), "Analysis and fabrication of patterned magnetorheological elastomers", *Smart Mater. Struct.*, **17**(4), p. 045001. https://doi.org/10.1088/0964-1726/17/4/045001

HJ